

In *itinere* infections covertly undermine localized epidemic control in metapopulations

Francesca Dilisante,^{1,2} Pablo Valgañón,^{1,3} David Soriano-Paños,^{4,1} and Jesús Gómez-Gardeñes^{1,2}

¹⁾*GOTHAM lab, Institute for Biocomputation and Physics of Complex Systems (BIFI), University of Zaragoza, 50018 Zaragoza (Spain).*

²⁾*Departament of Condensed Matter Physics, University of Zaragoza, 50009 Zaragoza (Spain).*

³⁾*Instituto Pirenaico de Ecología – CSIC, Avda. Montaña 1005, 50059 Zaragoza (Spain).*

⁴⁾*Departament de Matemàtiques i Enginyeria Informàtica, Universitat Rovira i Virgili,*

43007 Tarragona (Spain).

(Dated: 11 April 2025)

Metapopulation models have traditionally assessed epidemic dynamics by emphasizing local (*in situ*) interactions within defined subpopulations, often neglecting transmission occurring during mobility phases (*in itinere*). Here, we extend the Movement–Interaction–Return (MIR) metapopulation framework to explicitly include contagions acquired during transit, considering agents traveling along shared transportation networks. We reveal that incorporating *in itinere* contagion entails a notable reduction of the epidemic threshold and a pronounced delocalization of the epidemic trajectory, particularly significant in early-stage outbreaks.

Recent empirical evidence in the context of the COVID-19 pandemic^{1–3} indicates that individuals who regularly use mass transportation such as subways, trams, or buses face a significantly higher risk of contracting airborne diseases. In particular, for Influenza-like illnesses^{4,5}, the occurrence of infections among passengers increases with travel duration and seat proximity, suggesting that higher density and longer journeys amplify the risk of infection. Although many epidemic models incorporate human mobility and travel networks, they typically treat mobility as a single aggregate factor, without explicitly isolating infections acquired during transit. To address this limitation, we investigate how explicitly modeling the *in itinere* contagion route influences epidemic dynamics compared to frameworks that consider only *in situ* contagions. By leveraging a Markovian metapopulation formalism, we derive a mixing matrix that accounts for both *in situ* and *in itinere* infections in urban contexts. Equipped with this matrix, we show that *in itinere* contagions markedly affect the epidemic threshold and trigger a delocalization transition in early outbreaks—an outcome of paramount importance when designing targeted interventions.

I. INTRODUCTION

Epidemic modeling has long served as a cornerstone for understanding and mitigating the spread of infectious diseases since the early works by Ross⁶, which laid the groundwork for using mathematical approaches such as compartmental models^{7–9}. These frameworks, most notably the Susceptible–Infected–Recovered (SIR) model¹⁰, provided some of the earliest insights into epidemic dynamics, paving the way for practical forecasting tools. However, the inherent mean-field nature of these pioneering approaches overlooked the spatial and behavioral heterogeneities characteristic of real populations, limiting their applicability to qualitative agreement rather than quantitatively precise epidemic trajectories.

The advent of network theory^{11–13} and, more specifi-

cally, its application to metapopulation dynamics^{14–18}, enabled more realistic representations of population structure, wherein individuals interact within localized subpopulations (nodes) and move between them along well-defined mobility patterns. Metapopulation models, especially when coupled with agent-based simulations, have proven instrumental in investigating how human mobility¹⁹ critically shapes epidemic progression, enabling the global spread of disease from localized outbreaks across multiple geographical scales^{20–25}.

When considering metapopulation frameworks amenable to mathematical analysis, different mobility patterns can be modeled by coupling intra-node interactions with inter-node diffusion processes^{26–30}. In particular, frameworks incorporating recurrent mobility, mimicking daily commuting, have successfully captured urban epidemics^{31–33}. Yet, as noted in³⁴, a key challenge lies in accommodating complex social structures beyond the standard assumption that infections arise only *in situ* (within the nodes)—thus neglecting a vital transmission route: *in itinere* contagions, or those acquired during transit. In many real-world scenarios, especially airborne outbreaks such as COVID-19, this additional contagion mechanism^{1–5} has proven indispensable and, if ignored, may lead to underestimate the epidemic burden, ultimately affecting containment strategies.

In this work, we propose an extension to the metapopulation framework that explicitly incorporates what we refer to as *in itinere* contagions. Building upon the Movement–Interaction–Return (MIR) model^{33,35–39} with distinguishable agents^{40,41}, our approach introduces a third reaction phase accounting for contagions *in itinere*, i.e., while individuals travel between their residential and destination nodes. By extending the mixing matrix formalism^{40,41} to cover transit-based contacts, we derive an analytical expression for the epidemic threshold and show that disregarding *in itinere* contagions can overestimate population robustness and mischaracterize the epidemic detriment phenomenon observed in recurrent mobility settings.

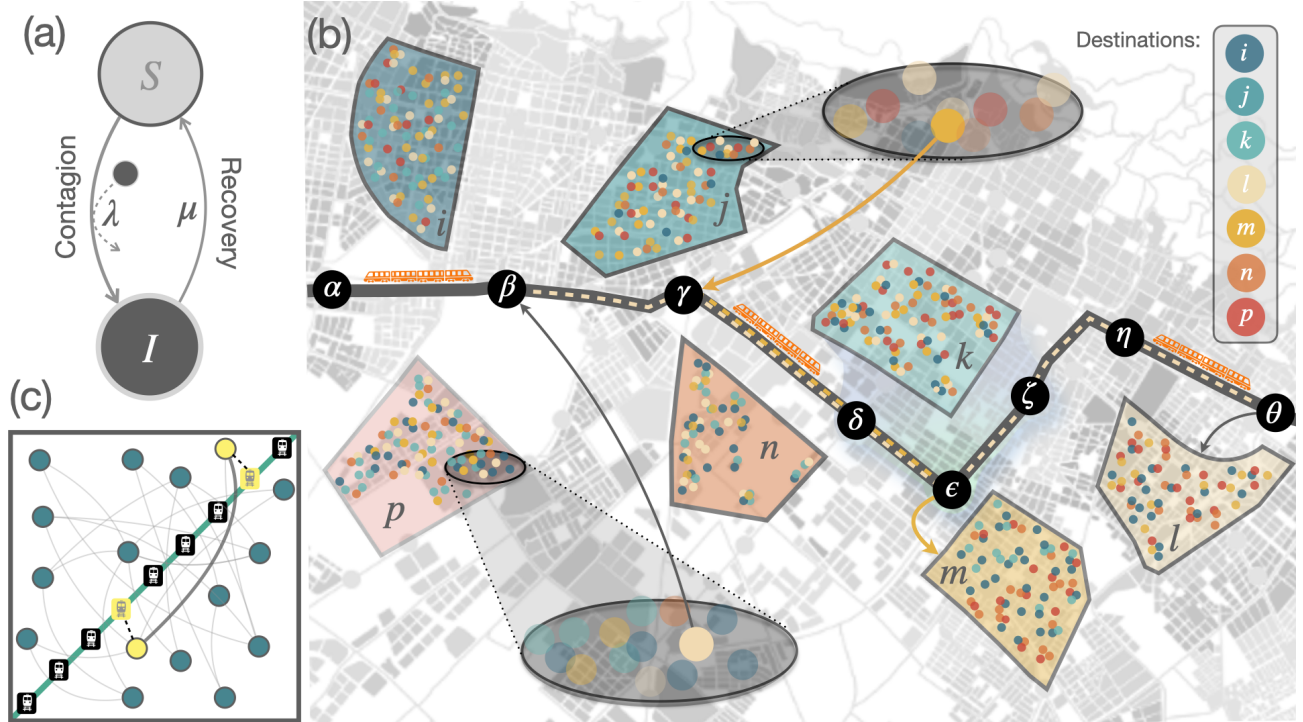


FIG. 1. Scheme of the metapopulation framework incorporating *in itinere* contagions. (a) Schematic representation of the SIS model. Individuals transition from the susceptible (S) to the infected (I) state with probability λ upon contact with an infectious individual, and recover to the susceptible state with probability μ . (b) Conceptual illustration of the distinguishable-agent MIR framework incorporating *in itinere* contagions. Polygons represent metapopulation nodes (e.g., i , j , k , etc.), with internal dots indicating residents, color-coded by their commuting destination. Black circles (α , β , γ , ...) denote transport stations connected by a transit line (black solid line). Dashed paths illustrate commuting transit routes: one from node j to m (yellow), and another from p to l (cream). Arrows indicate the boarding and alighting stations for each agent, with overlapping segments (e.g., $\gamma \rightarrow \epsilon$) representing shared exposure windows enabling *in itinere* transmission. This mechanism complements standard *in situ* interactions within nodes during day and night phases. (c) Scheme of the synthetic metapopulation model. Nodes are distributed and interconnected within a unit square, while a transport line with equidistant stations spans the diagonal. Boarding and alighting stations are assigned based on proximity between origin and destination nodes and the transport line (e.g. the two stations highlighted in yellow delimit the route followed by individuals commuting between the two nodes highlighted in yellow).

II. MODEL EQUATIONS

In this section, we present the MIR formulation that allows including *in itinere* contagions. To this aim, we first describe the MIR formalism to explain the basic features of the model and then introduce the possibility of contagions during transit.

A. MIR formalism with distinguishable agents

In its distinguishable formulation^{40,41}, the MIR model categorizes individuals not only by their place of residence but also by their usual destination. To support this formulation one usually relies on the Origin-Destination matrix, $\mathbf{n} = \{n_{ij}\}$, in which each element n_{ij} captures the total number of commuters from patch i to patch j for the population of interest. This matrix can be viewed as a directed and weighted network with L edges (the nonzero entries of \mathbf{n}).

Focusing (for simplicity) on the Susceptible-Infectious-Susceptible (SIS) compartmental model (see Fig. 1.a), the MIR formalism is described by $L \leq N^2$ variables, $\{\rho_{ij}(t)\}$,

where N denotes the number of patches in the metapopulation. In particular, each variable $\rho_{ij}(t)$ is the probability that an agent residing in node i and commuting to node j is infectious at time t . As is common in metapopulation models with recurrent mobility, these L variables $\{\rho_{ij}(t)\}$ evolve in discrete time steps. In particular, the Markovian update equation for an individual living in node i who commutes to node j reads:

$$\rho_{ij}(t+1) = (1 - \mu) \rho_{ij}(t) + (1 - \rho_{ij}(t)) \Pi_{ij}(t), \quad (1)$$

where μ is the SIS recovery probability, and $\Pi_{ij}(t)$ is the probability that a susceptible agent with residence i and destination j becomes infected during the current time step. As detailed below, $\Pi_{ij}(t)$ combines the contagion events that unfold across three sequential processes at each step. In particular, these processes are:

- 1. Movement (M):** At the beginning of each time step, individuals are placed in their residence node i . Then, with probability p_d , an individual travels to node j . Otherwise, with probability $1 - p_d$, the individual remains in node i .

- 2. Interaction (I):** Once at a node (either the residence i or destination j), each individual engages in local (*in situ*) contacts that can lead to infection. The contagion probability at node i during this *day* stage is:

$$P_i^D(t) = 1 - \left(1 - \lambda \frac{I_i^{\text{eff}}(t)}{n_i^{\text{eff}}}\right)^{z_D f_i}, \quad (2)$$

where λ is the per-contact infection probability of the SIS model, $I_i^{\text{eff}}(t)$ is the effective number of infected agents in node i after movement and n_i^{eff} is the node's effective population. Both quantities are defined as:

$$n_i^{\text{eff}} = (1 - p_d) \sum_j n_{ij} + p_d \sum_j n_{ji} \quad (3)$$

$$I_i^{\text{eff}}(t) = (1 - p_d) \sum_j n_{ij} \rho_{ij}(t) + p_d \sum_j n_{ji} \rho_{ji}(t). \quad (4)$$

In addition, $z_D = \langle k_D \rangle \sum_i n_i^{\text{eff}} / \sum_i f_i n_i^{\text{eff}}$ is a scaling factor ensuring an average of $\langle k_D \rangle$ day contacts, and $f_i = n_i^{\text{eff}} / a_i$ encodes the node's effective density (with a_i denoting its area). Note that agents infected during this day stage remain non-infectious until the following time step.

- 3. Return (R):** After the interaction phase, all individuals who traveled during the movement stage return to their home node to spend the *night* stage. There, they engage in additional contacts (e.g., household members) that may also result in infections. Being at home, the probability of these *in situ* contagions differs from Eq. ((2)):

$$P_i^N(t) = 1 - \left(1 - \lambda \rho_i(t)\right)^{\langle k_N \rangle}, \quad (5)$$

where $\rho_i(t)$ is the fraction of infected individuals in node i and $\langle k_N \rangle$ denotes the average number of night contacts in the population (assumed to be equal for all patches). As in the day phase, newly infected agents remain non-infectious until the next time step. Finally, those who were infectious during this time step recover with probability μ , thus entering the next time step as susceptible individuals.

B. Incorporating *In Itinere* Contagions

To capture the risk of infection while traveling, we introduce a third reaction component. When individuals decide to travel, they board a shared transportation network, interacting with other passengers along the way. We assume this network, composed of stations and connecting segments (see Fig. 1.b), is unique and universally used by all travellers. Each individual starts at the station nearest their residence and disembarks at the station closest to their destination. The route between these two stations (represented as a sequence of stretches between them) follows the shortest path⁴². Although certain

nodes (such as node k in Fig. 1.b) may have multiple equidistant stations, for simplicity, we associate one station with each node.

This expanded distinguishable MIR framework allows for interactions between individuals whose residences and workplaces do not overlap. For instance, consider in Fig. 1.b someone residing in node p and traveling to node l , boarding at station β and alighting at station θ . This person may interact with another traveler residing in node j and heading to node m while both are simultaneously aboard the transport network, that is, when their routes overlap. Note that, under the baseline MIR model, these individuals would have never encountered one another.

To capture this new transmission route into the mathematical formulation, we write the probability that an individual from node i traveling to node j becomes infected *in itinere* as:

$$P_{ij}^T(t) = 1 - \prod_{(\alpha,\beta)} \left(1 - \lambda \frac{I(\alpha,\beta)(t)}{n(\alpha,\beta)}\right)^{c(p_d) S_{ij}^{(\alpha,\beta)}}, \quad (6)$$

where $S_{ij}^{(\alpha,\beta)}$ is the (i,j) entry of matrix $\mathbf{S}^{(\alpha,\beta)}$, which encodes whether the path between nodes i and j includes the stretch (α,β) . Specifically, $S_{ij}^{(\alpha,\beta)} = 1$ if the route between i and j uses (α,β) , and 0 otherwise. Since the product $\prod_{(\alpha,\beta)}$ runs over all possible station-to-station stretches, the terms $S_{ij}^{(\alpha,\beta)}$ ensure that only those segments actually traveled by $(i \rightarrow j)$ affect $P_{ij}^T(t)$. Additionally, $n(\alpha,\beta)$ denotes the total number of individuals aboard on stretch (α,β) , which can be explicitly written as:

$$n(\alpha,\beta) = p_d \sum_{k,l} n_{kl} S_{kl}^{(\alpha,\beta)}, \quad (7)$$

where p_d scales the sum of all agents n_{kl} whose routes include (α,β) . Analogously, the number of infected individuals on that same stretch reads:

$$I(\alpha,\beta)(t) = p_d \sum_{k,l} n_{kl} \rho_{kl}(t) S_{kl}^{(\alpha,\beta)}. \quad (8)$$

Each traveler is assumed to make $c(p_d)$ contacts per stretch of the journey. This number is modeled using a first-order Hill equation:

$$c(p_d) = c_{\text{sat}} \frac{p_d}{K + p_d}, \quad (9)$$

so that, at low mobility p_d , the number of in-transit contacts remains small, whereas at higher mobility it grows asymptotically toward the saturation value c_{sat} .

Finally, considering the *in situ* infections during both day (Interaction) and night (Return) phases, along with this *in itinere* infection risk, the overall probability that a susceptible agent resident of node i who commutes to j becomes infected

in one time step is:

$$\Pi_{ij}(t) = (1 - p_d) \left[P_i^D(t) + \left(1 - P_i^D(t)\right) P_i^N(t) \right] + p_d \left[1 - \left(1 - P_{ij}^T(t)\right) \left(1 - P_j^D(t)\right) \left(1 - P_i^N(t)\right) \right]. \quad (10)$$

In this expression, the first term corresponds to individuals who do not travel (with probability $1 - p_d$) and thus encounter infection only in their residential node i . The second term, weighted by p_d , applies to those who travel to node j , factoring potential infections during transit, during the day at the destination, and during the night at home.

C. Mixing matrix and Epidemic threshold

The epidemic threshold, λ_c , is the smallest infection probability for which an endemic regime is attained. Therefore, to derive its value, we focus on the stationary states of the SIS dynamics near λ_c . In this regime, all variables are time-independent: $\rho_{ij}(t+1) = \rho_{ij}(t) = \rho_{ij}^*$ $\forall i, j$. Consequently, Eq. (1) simplifies to:

$$\mu \rho_{ij}^* = (1 - \rho_{ij}^*) \Pi_{ij}(\rho_{ij}^*). \quad (11)$$

Secondly, for $\lambda \gtrsim \lambda_c$, local prevalences are small: $\rho_{ij}^* = \varepsilon_{ij} \ll 1 \forall i, j$, enabling the linearization of Eq. (11). The linearized infection probabilities for the day, night, and in-transit reaction processes are:

$$P_i^D \approx p_d \lambda \frac{z^D f_i}{n_i^{eff}} \sum_{j=1}^N n_{ji} \varepsilon_{ji} + \lambda (1 - p_d) \frac{z^D f_i}{n_i^{eff}} \sum_{j=1}^N n_{ij} \varepsilon_{ij} \quad (12)$$

$$P_i^N \approx \lambda \frac{\langle k_N \rangle}{n_i} \sum_{j=1}^N n_{ij} \varepsilon_{ij} \quad (13)$$

$$P_{ij}^T \approx \lambda c(p_d) p_d \sum_{k,l} n_{lk} \varepsilon_{lk} \sum_{\alpha, \beta} \frac{S_{ij}^{(\alpha, \beta)} S_{lk}^{(\alpha, \beta)}}{n(\alpha, \beta)}. \quad (14)$$

Substituting these expressions into Eq. (10) yields a linearized form of $\Pi_{ij}(\vec{\rho}^*)$, which, when inserted into Eq. (11) and neglecting nonlinear terms in ε_{ij} , leads to the following set of equations for the stationary local prevalence:

$$\mu \varepsilon_{ij} \approx \Pi_{ij}(\vec{\varepsilon}) = \lambda \sum_{k,l} M_{jk}^{il} \varepsilon_{lk}. \quad (15)$$

For convenience, in the former expression $\Pi_{ij}(\vec{\varepsilon})$ has been expressed as the product of the stationary prevalence vector $\vec{\varepsilon}$ and the so-called mixing matrix^{40,41} \mathbf{M} , whose element M_{jk}^{il} encodes how individuals with residence i and destination j

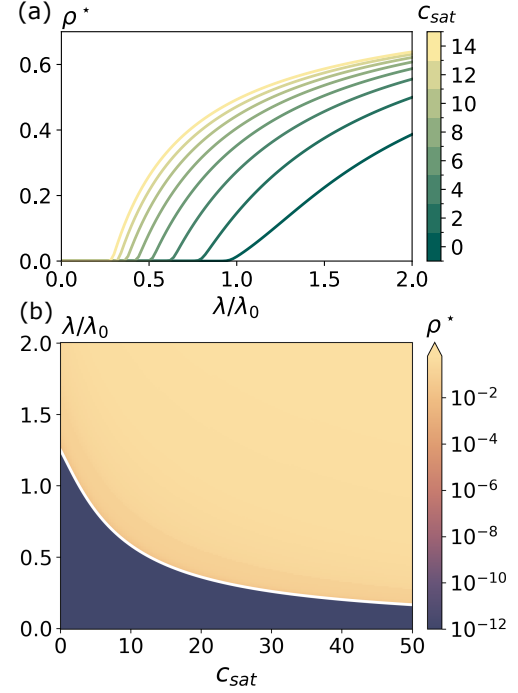


FIG. 2. Effect of c_{sat} on epidemic impact and threshold. (a) Steady-state fraction of infected individuals, ρ^* , as a function of the normalized infection probability λ/λ_0 , where λ_0 is the epidemic threshold at $p_d = 0$. Results are shown for $p_d = 0.3$ and various c_{sat} values. (b) Epidemic phase diagram $\rho^*(\lambda/\lambda_0, c_{sat})$ at $p_d = 0.3$, illustrating the dependence of disease prevalence ρ^* on λ/λ_0 and c_{sat} . The solid white line represents the epidemic threshold, λ_c/λ_0 , obtained from Eq. (17). We have set $K = 10^{-3}$, $\langle k_D \rangle = 8$ and $\langle k_N \rangle = 3$.

interact with those with residence l and destination k :

$$\begin{aligned} M_{jk}^{il} = & (1 - p_d) p_d \frac{z^D f_k}{n_k^{eff}} n_{lk} \delta_{ik} + (1 - p_d)^2 \frac{z^D f_l}{n_l^{eff}} n_{lk} \delta_{il} \\ & + p_d^2 \frac{z^D f_k}{n_k^{eff}} n_{lk} \delta_{jk} + p_d (1 - p_d) \frac{z^D f_l}{n_l^{eff}} n_{lk} \delta_{jl} + \frac{\langle k_N \rangle}{n_l} n_{lk} \delta_{il} \\ & + p_d^2 c(p_d) n_{lk} \sum_{\alpha, \beta} \frac{S_{ij}^{(\alpha, \beta)} S_{lk}^{(\alpha, \beta)}}{n(\alpha, \beta)}. \end{aligned} \quad (16)$$

Note that while the first five terms account for *in situ* encounters (and correspond to those present in the purely distinguishable-agent mixing matrix framework⁴⁰), the last one captures in-transit interactions.

Finally, turning our attention to Eq. (15), it is clear that given \mathbf{M} this equation can be written as an eigenvalue problem: $(\mu/\lambda) \cdot \vec{\varepsilon} = \mathbf{M} \vec{\varepsilon}$. Thus, since we are interested in the minimum value of λ fulfilling the former expression, the epidemic threshold reads:

$$\lambda_c = \frac{\mu}{\Lambda_{max}(\mathbf{M})}, \quad (17)$$

where $\Lambda_{max}(\mathbf{M})$ is the spectral radius of the mixing matrix.

III. RESULTS

To assess the impact of *in itinere* contagions, we employ a synthetic metapopulation structure with $N = 100$ nodes and average degree $\langle k \rangle = 19$. The nodes have randomly assigned populations averaging $\langle n_i \rangle = 500$, and the edges' weights, n_{ij} , are also randomly assigned: a random fraction of each node's population will travel to each of its available destinations. In addition, nodes are spatially distributed within a unit square, interconnected by a transport network composed of $N_T = 9$ equidistant stations placed along the diagonal, facilitating bidirectional commuting. In Fig. 1.c we show a schematic plot of the former metapopulation structure.

Leveraging this synthetic metapopulation with an integrated transport network, our numerical simulations reveal that explicitly modeling *in itinere* infections notably increases the steady-state disease prevalence ρ^* , particularly as the in-transit contact parameter c_{sat} rises (see Fig. 2.a). Furthermore, the epidemic threshold λ_c significantly decreases with increasing c_{sat} , highlighting that ignoring transit-based infections leads to substantial underestimations of the epidemic risk. Analytical predictions derived from Eq. (17) align remarkably with numerical results (see Fig. 2.b), validating the proposed mixing matrix formulation as a powerful analytical tool for assessing the resilience of populations against infectious disease outbreaks. Note that in this latter plot we use λ_0 , the critical threshold at $p_d = 0$, as a normalization factor for λ to focus on the effect of the transit contacts on the threshold.

Prior implementations of the MIR formalism have revealed the so-called epidemic detriment phenomenon i.e. an increase in the epidemic threshold, λ_c , for $p_d \gtrsim 0$ relative to the null mobility scenario ($p_d = 0$). Although it may initially seem counterintuitive, this effect can be understood by considering the case $p_d = 0$, $\lambda \gtrsim \lambda_0$, where the majority of infections are concentrated within the most vulnerable patch of the metapopulation. When mobility is introduced at a low level, infected individuals can travel to less vulnerable, disease-free patches where the pathogen cannot generate a local outbreak. Concurrently, individuals entering the most affected patch are predominantly healthy, thereby further diluting the disease's prevalence in that patch. As a result, the localized outbreak in the most vulnerable patch can subside without triggering secondary infections in more sparsely populated patches, effectively increasing the epidemic threshold λ_c .

Let us note that, within this formalism, in the null mobility scenario ($p_d = 0$) the most vulnerable patch is the one where most contacts occur per time step: $z^D f_{max} + \langle k_N \rangle$, that is, the one that is most densely populated. In our synthetic metapopulation, all nodes have been assigned the same area, meaning that the most vulnerable patch is the most populated one at low mobility.

Remarkably, the inclusion of *in itinere* contagions counteracts the -otherwise seemingly robust- epidemic detriment phenomenon. Figure 3.a shows the relationship between λ_c/λ_0 and p_d for increasing values of c_{sat} . This figure reveals how in-transit contagion not only reduces the epidemic threshold but also plays a pivotal role in mitigating epidemic detri-

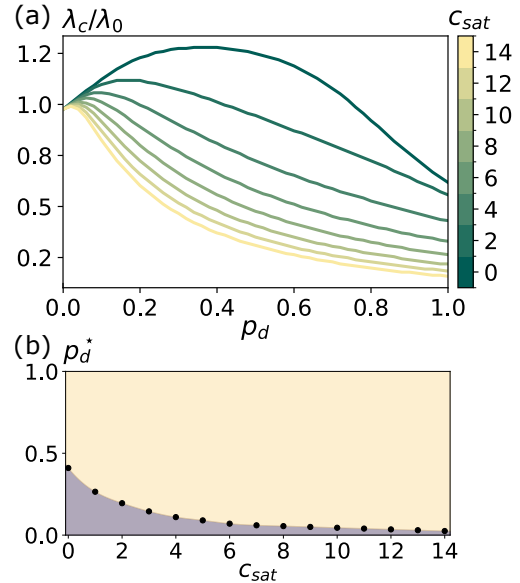


FIG. 3. Impact of c_{sat} on the epidemic detriment phenomenon. (a) Normalized epidemic threshold λ_c/λ_0 as a function of mobility p_d , where λ_0 denotes the epidemic threshold in the absence of mobility ($p_d = 0$). Results for various c_{sat} values are represented, showcasing how in-transit contacts modulate the critical conditions for epidemic onset. (b) Mobility value p_d^* , defined as the value of p_d that maximizes the epidemic threshold λ_c , plotted against c_{sat} . The shaded regions distinguish regimes where increasing mobility increases λ_c (light purple) from those where it decreases it (light yellow). Simulations consider $K = 10^{-3}$, $\langle k_D \rangle = 8$, and $\langle k_N \rangle = 3$.

ment. As the number of in-transit contacts increases, this phenomenon is progressively countered, eventually nearly disappearing altogether, as evidenced by the decrease in p_d^* (the mobility value at which λ_c reaches its maximum) with increasing c_{sat} (see Fig. 3.b). In the SM, we analytically derive the inverse dependence of p_d^* through a perturbative analysis of the mixing matrix \mathbf{M} .

To determine the effect of *in itinere* contagion on disease localization in the population, we compute the inverse participation ratio (IPR) as a function of mobility, p_d , and the per-segment in-transit contacts, c_{sat} . The IPR has proven to be a good indicator for localization in spreading dynamics on complex networks^{35,43,44}. Since we aim to quantify the contribution of each patch to the overall outbreak, we first coarse grain the maximum eigenvector, $\varepsilon_{max}(\mathbf{M})$, by summing the contributions associated to each patch i , yielding a new eigenvector with N entries, \mathbf{V}_{max} :

$$(\mathbf{V}_{max})_i = \frac{\sum_{j=1}^N \varepsilon_{ij}^{max}}{\sqrt{\sum_{k=1}^N [\sum_{j=1}^N \varepsilon_{ij}^{max}]^2}}. \quad (18)$$

The IPR is then defined as:

$$\text{IPR} = \sum_{i=1}^N (\mathbf{V}_{max})_i^4. \quad (19)$$

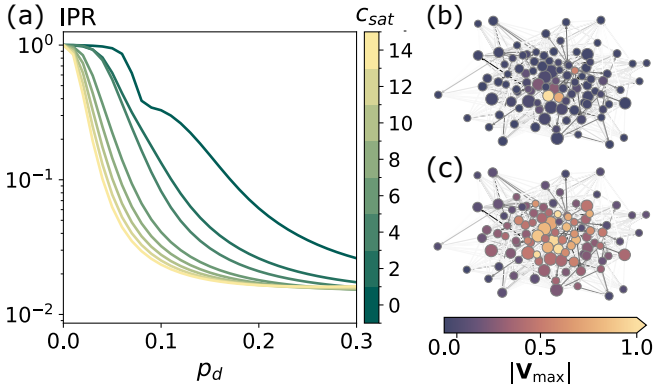


FIG. 4. Correlation between c_{sat} and the epidemic delocalization. (a) Inverse Participation Ratio (IPR) as a function of mobility, p_d , for several c_{sat} values. (b)-(c) Metapopulation network representations for $p_d = 0.1$ at $c_{sat} = 0$ (panel (b)) and $c_{sat} = 14$ (panel (c)). Node sizes are proportional to the population of each patch, link colors (ranging from white to black) reflect the corresponding n_{ij} values in the OD matrix, and node colors represent the components of the coarse-grained maximum eigenvector \mathbf{V}_{max} , capturing the localization of the infection. Simulations consider $K = 10^{-3}$, $\langle k_D \rangle = 8$ and $\langle k_N \rangle = 3$.

This quantity is bounded between $1/N$ (fully delocalized, where all patches contribute equally to the epidemic) and 1 (fully localized, where infections are confined to a single patch).

As demonstrated in Fig. 4.a, for all values of c_{sat} , an increase in p_d results in a decrease in the IPR, pinpointing a delocalization transition driven by geographical mixing due to mobility. Furthermore, as c_{sat} increases, this transition occurs at lower p_d , emphasizing the pivotal role of in-transit contacts in driving early delocalization. These contacts contribute to disease homogenization through two main mechanisms: (i) increasing the total number of contacts and (ii) enabling interactions between individuals who neither share their residence nor destination—interactions that do not occur in the baseline MIR model. Additionally, Figs. 4.b-c schematically depict the metapopulation, with patches color-coded by their corresponding element in the \mathbf{V}_{max} vector. This visualization further illustrates that, for fixed mobility ($p_d = 0.1$), increasing in-transit contacts (c_{sat}) leads to epidemic delocalization. In this context, c_{sat} governs a transition in the infection distribution from a localized state—confined to a few patches—to a widespread and homogeneous state across the network. Our findings thus represent a cautionary tale for the implementation of targeted strategies, as the delocalization of epidemic states driven by in-transit contagions substantially reduce their suitability as a control strategy to mitigate epidemic outbreaks.

IV. CONCLUSIONS

In this work, we have proposed a metapopulation framework introducing a novel mechanism that accounts for conta-

gion events occurring during individual transit across a shared transportation infrastructure. By incorporating in-itineri contagions into the MIR modeling scheme, we have revealed a non-negligible transmission route that substantially alters both the epidemic threshold and the spatial progression of outbreaks. This refinement provides a more faithful representation of disease dynamics in urban environments, particularly for airborne pathogens.

The analytical derivation of the mixing matrix, which now includes terms representing in-transit contacts, enables a precise characterization of the epidemic threshold through spectral analysis. Numerical simulations, conducted on a synthetic yet structurally realistic metapopulation, confirm that in-itineri contagions lead to a significant reduction in the epidemic threshold and an increase in disease prevalence. Moreover, we have shown that the presence of transit-based infections progressively diminishes the epidemic detriment phenomenon, thereby reshaping the critical conditions under which mobility enhances or suppresses epidemic spread.

Beyond the epidemic onset, we have also demonstrated that in-itineri contagions are a potent driver of epidemic delocalization. Using the inverse participation ratio as a metric for localization, we have shown that increased transit contacts precipitate a rapid transition from localized to widespread infection states. This finding highlights a fundamental shift in the spatial profile of outbreaks, whereby infections are no longer confined to highly vulnerable patches but become uniformly distributed across the metapopulation.

Overall, our results underscore that ignoring in-itineri contagions may lead to significant underestimations of epidemic severity and mischaracterization of spatial dynamics, thereby compromising the design and effectiveness of containment strategies. The framework developed here can be readily adapted to empirical mobility and transportation data, paving the way for more accurate scenario analyses and targeted intervention policies.

ACKNOWLEDGEMENTS

F.D. and J.G.-G. acknowledge support from Departamento de Industria e Innovación del Gobierno de Aragón y Fondo Social Europeo (FENOL group Grant No. E36-23R) and Ministerio de Ciencia e Innovación (Grants No. PID2020-113582GB-I00 and No. PID2023-147734NB-I00). D.S.-P. acknowledges financial support through grants JDC2022-048339-I and PID2021-128005NB-C21 funded by MCIN/AEI/10.13039/501100011033 and the European Union “NextGenerationEU”/PRTR”.

REFERENCES

¹M. Hu, H. Lin, J. Wang, C. Xu, A. J. Tatem, B. Meng, X. Zhang, Y. Liu, P. Wang, G. Wu, H. Xie, and S. Lai, “Risk of coronavirus disease 2019 transmission in train passengers: an epidemiological and modeling study,” Clinical Infectious Dis-

- eases **72**, 604–610 (2020), <https://academic.oup.com/cid/article-pdf/72/4/604/36272534/ciaa1057.pdf>.
- ²P. Li, X. Chen, C. Ma, C. Zhu, and W. Lu, “Risk assessment of covid-19 infection for subway commuters integrating dynamic changes in passenger numbers,” *Environmental Science and Pollution Research* **29**, 74715–74724 (2022).
- ³L. Tapiador, J. Gomez, and J. M. Vassallo, “Exploring the relationship between public transport use and covid-19 infection: A survey data analysis in madrid region,” *Sustainable Cities and Society* **104**, 105279 (2024).
- ⁴J. Troko, P. Myles, J. Gibson, A. Hashim, J. Enstone, S. Kingdon, C. Packham, S. Amin, A. Hayward, and J. N. Van-Tam, “Is public transport a risk factor for acute respiratory infection?” *BMC Infectious Diseases* **11**, 16 (2011).
- ⁵L. Goscé and A. Johansson, “Analysing the link between public transport use and airborne transmission: mobility and contagion in the london underground,” *Environmental Health* **17**, 84 (2018).
- ⁶R. Ross, *The Prevention of Malaria* (John Murray, London, 1911).
- ⁷N. T. Bailey, “The mathematical theory of epidemics,” Tech. Rep. (1957).
- ⁸R. M. Anderson and R. M. May, *Infectious Diseases of Humans: Dynamics and Control* (Oxford University Press, 1992).
- ⁹G. P. Wormser and B. Pourbohloul, “Modeling infectious diseases in humans and animals by matthew james keeling and pejman rohani princeton, nj: Princeton university press, 2008. 408 pp.” (2008).
- ¹⁰W. O. Kermack and A. G. McKendrick, “A contribution to the mathematical theory of epidemics,” *Proceedings of the royal society of london. Series A, Containing papers of a mathematical and physical character* **115**, 700–721 (1927).
- ¹¹R. Pastor-Satorras, C. Castellano, P. Van Mieghem, and A. Vespignani, “Epidemic processes in complex networks,” *Reviews of Modern Physics* **87**, 925 (2015).
- ¹²W. Wang, M. Tang, H. E. Stanley, and L. A. Braunstein, “Unification of theoretical approaches for epidemic spreading on complex networks,” *Reports on Progress in Physics* **80**, 036603 (2017).
- ¹³C. Granell, S. Gómez, J. Gómez-Gardeñes, and A. Arenas, “Probabilistic discrete-time models for spreading processes in complex networks: A review,” *Annalen der Physik* **536**, 2400078 (2024), <https://onlinelibrary.wiley.com/doi/pdf/10.1002/andp.202400078>.
- ¹⁴V. Colizza, R. Pastor-Satorras, and A. Vespignani, “Reaction-diffusion processes and metapopulation models in heterogeneous networks,” *Nature Physics* **3**, 276–282 (2007).
- ¹⁵V. Colizza and A. Vespignani, “Epidemic modeling in metapopulation systems with heterogeneous coupling pattern: Theory and simulations,” *Journal of Theoretical Biology* **251**, 450–467 (2008).
- ¹⁶V. Colizza and A. Vespignani, “Invasion threshold in heterogeneous metapopulation networks,” *Phys. Rev. Lett.* **99**, 148701 (2007).
- ¹⁷D. Balcan, V. Colizza, B. Gonçalves, H. Hu, J. J. Ramasco, and A. Vespignani, “Multiscale mobility networks and the spatial spreading of infectious diseases,” *Proceedings of the National Academy of Sciences* **106**, 21484–21489 (2009).
- ¹⁸M. Tizzoni, P. Bajardi, A. Decuyper, G. Kon Kam King, C. M. Schneider, V. Blondel, Z. Smoreda, M. C. González, and V. Colizza, “On the use of human mobility proxies for modeling epidemics,” *PLoS Computational Biology* **10**, e1003716 (2014).
- ¹⁹H. Barbosa, M. Barthelemy, G. Ghoshal, C. R. James, M. Lenormand, T. Louail, R. Menezes, J. J. Ramasco, F. Simini, and M. Tommasini, “Human mobility: Models and applications,” *Physics Reports* **734**, 1–74 (2018).
- ²⁰S. Ebank, H. Guclu, V. S. Anil Kumar, M. V. Marathe, A. Srinivasan, Z. Toroczkai, and N. Wang, “Modelling disease outbreaks in realistic urban social networks,” *Nature* **429**, 180–184 (2004).
- ²¹V. Colizza, M. Barthélémy, A. Barrat, and A. Vespignani, “Epidemic modeling in complex realities,” *Comptes Rendus Biologies* **330**, 364–374 (2007).
- ²²D. Balcan, B. Gonçalves, H. Hu, J. J. Ramasco, V. Colizza, and A. Vespignani, “Modeling the spatial spread of infectious diseases: The global epidemic and mobility computational model,” *Journal of Computational Science* **1**, 132–145 (2010).
- ²³M. Ajelli, B. Gonçalves, D. Balcan, V. Colizza, H. Hu, J. Ramasco, S. Merler, and A. Vespignani, “Comparing large-scale computational approaches to epidemic modeling: Agent-based versus structured metapopulation models,” *BMC Infectious Diseases* **10**, 190 (2010).
- ²⁴M. Tizzoni, P. Bajardi, C. Poletto, J. J. Ramasco, D. Balcan, B. Gonçalves, N. Perra, V. Colizza, and A. Vespignani, “Real-time numerical forecast of global epidemic spreading: case study of 2009 a/h1n1pdm,” *BMC Medicine* **10**, 1–31 (2012).
- ²⁵M. Chinazzi, J. T. Davis, M. Ajelli, C. Gioannini, M. Litvinova, S. Merler, A. P. y Piontti, K. Mu, L. Rossi, K. Sun, C. Viboud, X. Xiong, H. Yu, M. E. Halloran, I. M. Longini, and A. Vespignani, “The effect of travel restrictions on the spread of the 2019 novel coronavirus (covid-19) outbreak,” *Science* **368**, 395–400 (2020).
- ²⁶D. Brockmann and D. Helbing, “The hidden geometry of complex, network-driven contagion phenomena,” *Science* **342**, 1337–1342 (2013).
- ²⁷N. Masuda, “Effects of diffusion rates on epidemic spreads in metapopulation networks,” *New Journal of Physics* **12**, 093009 (2010).
- ²⁸C. Poletto, M. Tizzoni, and V. Colizza, “Human mobility and time spent at destination: Impact on spatial epidemic spreading,” *Journal of Theoretical Biology* **338**, 41–58 (2013).
- ²⁹A. Apolloni, C. Poletto, J. Ramasco, P. Jensen, and V. Colizza, “Metapopulation epidemic models with heterogeneous mixing and travel behaviour,” *Theoretical Biology and Medical Modelling* **11**, 3 (2014).
- ³⁰P. Castioni, R. Gallotti, and M. De Domenico, “Critical behavior in interdependent spatial spreading processes with distinct characteristic time scales,” *Communications Physics* **4**, 131 (2021).
- ³¹D. Balcan and A. Vespignani, “Phase transitions in contagion processes mediated by recurrent mobility patterns,” *Nature physics* **7**, 581–586 (2011).
- ³²V. Belik, T. Geisel, and D. Brockmann, “Natural human mobility patterns and spatial spread of infectious diseases,” *Physical Review X* **1**, 011001 (2011).
- ³³J. Gómez-Gardeñes, D. Soriano-Paños, and A. Arenas, “Critical regimes driven by recurrent mobility patterns of reaction–diffusion processes in networks,” *Nature Physics* **14**, 391–395 (2018).
- ³⁴F. Ball, T. Britton, T. House, V. Isham, D. Mollison, L. Pellis, and G. Scalia Tomba, “Seven challenges for metapopulation models of epidemics, including households models,” *Epidemics* **10**, 63–67 (2015), challenges in Modelling Infectious Disease Dynamics.
- ³⁵D. Soriano-Paños, L. Lotero, A. Arenas, and J. Gómez-Gardeñes, “Spreading processes in multiplex metapopulations containing different mobility networks,” *Physical Review X* **8**, 031039 (2018).
- ³⁶D. Soriano-Paños, J. H. Arias-Castro, A. Reyna-Lara, H. J. Martínez, S. Meloni, and J. Gómez-Gardeñes, “Vector-borne epidemics driven by human mobility,” *Phys. Rev. Res.* **2**, 013312 (2020).
- ³⁷W. Cota, D. Soriano-Paños, A. Arenas, S. C. Ferreira, and J. Gómez-Gardeñes, “Infectious disease dynamics in metapopulations with heterogeneous transmission and recurrent mobility,” *New Journal of Physics* **23**, 073019 (2021).
- ³⁸S. Haze, D. Soriano-Paños, A. Arenas, J. Gómez-Gardeñes, and G. Ghoshal, “Interplay between population density and mobility in determining the spread of epidemics in cities,” *Communications Physics* **4**, 1–10 (2021).
- ³⁹D. Soriano-Paños, W. Cota, S. C. Ferreira, G. Ghoshal, A. Arenas, and J. Gómez-Gardeñes, “Modeling communicable diseases, human mobility, and epidemics: A review,” *Annalen der Physik* **534**, 2100482 (2022).
- ⁴⁰P. Valgañón, D. Soriano-Paños, A. Arenas, and J. Gómez-Gardeñes, “Contagion–diffusion processes with recurrent mobility patterns of distinguishable agents,” *Chaos: An Interdisciplinary Journal of Nonlinear Science* **32**, 043102 (2022), https://pubs.aip.org/aip/cha/article-pdf/doi/10.1063/5.0085532/16451730/043102_1_online.pdf.
- ⁴¹P. Valgañón, A. F. Useche, F. Montes, A. Arenas, D. Soriano-Paños, and J. Gómez-Gardeñes, “Human behavior-driven epidemic surveillance in urban landscapes,” *npj Complexity* **1**, 21 (2024).
- ⁴²V. Latora, V. Nicosia, and G. Russo, *Complex Networks: Principles, Methods and Applications* (Cambridge University Press, 2017).
- ⁴³A. V. Goltsev, S. N. Dorogovtsev, J. G. Oliveira, and J. F. F. Mendes, “Localization and spreading of diseases in complex networks,” *Phys. Rev. Lett.* **109**, 128702 (2012).
- ⁴⁴T. Martin, X. Zhang, and M. E. J. Newman, “Localization and centrality in networks,” *Phys. Rev. E* **90**, 052808 (2014).
- ⁴⁵R. A. Marcus, “Brief comments on perturbation theory of a nonsymmetric matrix: The gf matrix,” *The Journal of Physical Chemistry A* **105**, 2612–2616 (2001).

SUPPLEMENTARY MATERIAL: *IN ITINERE* INFECTIONS COVERTLY UNDERMINE LOCALIZED EPIDEMIC CONTROL IN METAPOPULATIONS

A perturbative approach to evaluating the epidemic threshold and analyzing the effect of *in itinere* contagion on the epidemic detriment phenomenon.

The analytical expression for the epidemic threshold, given in Eq. (15) of the main text, requires the knowledge of the largest eigenvalue of the mixing matrix \mathbf{M} . Since a closed-form expression for the eigenvalues of \mathbf{M} is not generally available, we compute them via numerical diagonalization. However, in the low-mobility regime ($p_d \approx 0$), perturbation theory provides a valid approximation for the spectral radius of the mixing matrix^{33,45}, thus enabling the derivation of an analytical expression for the epidemic threshold. This approach offers insight into the behavior of λ_c in this regime. Note that, to avoid notational ambiguity, in this supplementary material we denote the epidemic threshold by λ_c .

Starting from the mixing matrix defined in Eq. (14) of the main text, we reorganize its terms according to powers of p_d . Thus, introducing $n'(\alpha, \beta) = \frac{n(\alpha, \beta)}{p_d}$ and $T_{jk}^{il} = \sum_{\alpha, \beta} \frac{S_{ij}^{(\alpha, \beta)} S_{lk}^{(\alpha, \beta)}}{n'(\alpha, \beta)}$ we arrive at:

$$\begin{aligned} (\mathbf{M}_{jk}^{il})^T = & \left(\frac{z^D f_l}{n_l^{eff}} + \frac{\langle k_N \rangle}{n_l} \right) n_{lk} \delta_{li} + \\ & p_d \left[\frac{z^D f_k}{n_k^{eff}} \delta_{ki} + \frac{z^D f_l}{n_l^{eff}} (-2\delta_{li} + \delta_{lj}) + c T_{jk}^{il} \right] n_{lk} + \\ & p_d^2 \left[\frac{z^D f_k}{n_k^{eff}} (\delta_{kj} - \delta_{ki}) + \frac{z^D f_l}{n_l^{eff}} (\delta_{li} + \delta_{lj}) \right] n_{lk}. \end{aligned} \quad (\text{S.1})$$

To derive Eq. (S.1), we have also considered that the number of in-transit contacts $c(p_d) = c_{sat} \frac{p_d}{K+p_d} \approx c_{sat}$ for $K \ll p_d$, a valid assumption for the values considered in our simulations $K = 10^{-3}$.

Additionally, in order to work with a $N^2 \times N^2$ matrix, we adopt the compact notation $M_{lk}^{ij} = M_{l:N+k}^{i:N+j}$ and, given the decomposition of the mixing matrix into powers of p_d , we express it as:

$$\mathbf{M} = \mathbf{M}_0 + p_d \mathbf{M}_1 + p_d^2 \mathbf{M}_2. \quad (\text{S.2})$$

where \mathbf{M}_0 represents the unperturbed matrix, and \mathbf{M}_1 and \mathbf{M}_2 correspond to the first- and second-order perturbative corrections, respectively.

Following perturbation theory, the eigenvalues and eigenvectors of the mixing matrix \mathbf{M} can be expressed as power series in p_d :

$$\begin{aligned} \Lambda^i(p_d) &= \Lambda_0^i + p_d \Lambda_1^i + p_d^2 \Lambda_2^i + \dots \\ |\Psi_i\rangle &= |0\rangle + p_d |1\rangle + p_d^2 |2\rangle + \dots \end{aligned} \quad (\text{S.3})$$

At zeroth order, the eigenvalues are given by:

$$\Lambda_0^i = \Lambda^i(\mathbf{M}_0), \quad (\text{S.4})$$

where $\Lambda^i(\mathbf{M}_0)$ denotes the i -th eigenvalue of the unperturbed matrix \mathbf{M}_0 .

In the present formalism, the structure of \mathbf{M}_0 is:

$$(\mathbf{M}_0)_{l:N+k}^{i:N+j} = \left(\frac{z^D f_l}{n_l^{eff}} + \frac{\langle k_N \rangle}{n_l} \right) n_{lk} \delta_{li}, \quad (\text{S.5})$$

which is block-diagonal. The blocks are:

$$(\mathbf{M}_0)_i^i = \left(\frac{z^D f_i}{n_i^{eff}} + \frac{\langle k_N \rangle}{n_i} \right) \begin{pmatrix} n_{i1} & n_{i2} & \dots & n_{iN} \\ n_{i1} & n_{i2} & \dots & n_{iN} \\ \vdots & \vdots & \ddots & \vdots \\ n_{i1} & n_{i2} & \dots & n_{iN} \end{pmatrix}. \quad (\text{S.6})$$

This block structure is equivalent to an $N \times N$ matrix with identical rows:

$$\mathbf{A} = \begin{pmatrix} a_1 & a_2 & \dots & a_N \\ a_1 & a_2 & \dots & a_N \\ \vdots & \vdots & \ddots & \vdots \\ a_1 & a_2 & \dots & a_N \end{pmatrix}. \quad (\text{S.7})$$

Such a matrix has the following well-known spectral properties:

1. Its largest eigenvalue is $\Lambda_{\max} = \sum_i a_i$, with associated eigenvector:

$$|v\rangle = \begin{pmatrix} 1 \\ 1 \\ \vdots \\ 1 \end{pmatrix}.$$

2. All other eigenvalues are zero, with a degeneracy of $N - 1$.

Proof. To verify that $|v\rangle$ is an eigenvector of \mathbf{A} with eigenvalue $\Lambda = \sum_i a_i$, we compute:

$$\mathbf{A} \cdot |v\rangle = \begin{pmatrix} a_1 & a_2 & \dots & a_N \\ a_1 & a_2 & \dots & a_N \\ \vdots & \vdots & \ddots & \vdots \\ a_1 & a_2 & \dots & a_N \end{pmatrix} \begin{pmatrix} 1 \\ 1 \\ \vdots \\ 1 \end{pmatrix} = \left(\sum_{i=1}^N a_i \right) \begin{pmatrix} 1 \\ 1 \\ \vdots \\ 1 \end{pmatrix}.$$

To confirm that 0 is also an eigenvalue, we consider any vector $|x\rangle$ orthogonal to $|v\rangle$:

$$\mathbf{A} \cdot |x\rangle = 0,$$

which implies:

$$\sum_{j=1}^N a_j x_j = 0.$$

There exist $N - 1$ linearly independent solutions to this equation, forming a basis for the $N - 1$ -dimensional subspace associated with eigenvalue 0. For instance, we can construct eigenvectors of the form:

$$\begin{pmatrix} -1/a_1 \\ 1/a_2 \\ 0 \\ \vdots \\ 0 \end{pmatrix}, \quad \begin{pmatrix} -1/a_1 \\ 0 \\ 1/a_3 \\ \vdots \\ 0 \end{pmatrix}, \quad \dots, \quad \begin{pmatrix} -1/a_1 \\ 0 \\ 0 \\ \vdots \\ 1/a_N \end{pmatrix}.$$

This confirms that the eigenvalue 0 has multiplicity $N - 1$, and thus $\Lambda = \sum_i a_i$ is the unique maximum eigenvalue. ■

Similarly, the left eigenvectors and eigenvalues of the matrix \mathbf{A} can be obtained as the right eigenvectors and eigenvalues of its transpose, \mathbf{A}^T :

$$\mathbf{A}^T = \begin{pmatrix} a_1 & a_1 & \dots & a_1 \\ a_2 & a_2 & \dots & a_2 \\ \vdots & \vdots & \ddots & \vdots \\ a_N & a_N & \dots & a_N \end{pmatrix}. \quad (\text{S.8})$$

In this case, all columns are identical. Consequently, the matrix \mathbf{A}^T satisfies the following spectral properties:

1. Its largest eigenvalue is $\Lambda_{\max} = \sum_i a_i$, with associated eigenvector

$$|v\rangle = \begin{pmatrix} a_1 \\ a_2 \\ \vdots \\ a_N \end{pmatrix}.$$

2. The only other eigenvalue is 0, with degeneracy $N - 1$.

Proof. We first verify that $|v\rangle = (a_1, a_2, \dots, a_N)^T$ is an eigenvector of \mathbf{A}^T with eigenvalue $\Lambda = \sum_i a_i$:

$$\mathbf{A}^T \cdot |v\rangle = \begin{pmatrix} a_1 & a_1 & \dots & a_1 \\ a_2 & a_2 & \dots & a_2 \\ \vdots & \vdots & \ddots & \vdots \\ a_N & a_N & \dots & a_N \end{pmatrix} \begin{pmatrix} a_1 \\ a_2 \\ \vdots \\ a_N \end{pmatrix} = \left(\sum_{i=1}^N a_i \right) \begin{pmatrix} a_1 \\ a_2 \\ \vdots \\ a_N \end{pmatrix}.$$

To show that 0 is an eigenvalue, we consider any vector $|x\rangle$ such that:

$$\mathbf{A}^T \cdot |x\rangle = \vec{a} \cdot \sum_{j=1}^N x_j \mathbf{e}_j = \mathbf{0} \implies \sum_{j=1}^N x_j = 0.$$

There exist $N - 1$ linearly independent solutions to this constraint, forming a basis for the subspace corresponding to eigenvalue 0. One possible choice of such eigenvectors is:

$$\begin{pmatrix} -1 \\ 1 \\ 0 \\ \vdots \\ 0 \end{pmatrix}, \quad \begin{pmatrix} -1 \\ 0 \\ 1 \\ \vdots \\ 0 \end{pmatrix}, \quad \dots, \quad \begin{pmatrix} -1 \\ 0 \\ 0 \\ \vdots \\ 1 \end{pmatrix}.$$

Therefore, the eigenvalue $\Lambda = \sum_i a_i$ is the unique nonzero eigenvalue and corresponds to the principal eigenvector of \mathbf{A}^T . ■

Applying these results to the mixing matrix blocks, $(\mathbf{M}_0)_i^i$, we have that for each block i the largest eigenvalue is:

$$\Lambda_0^i = \left(\frac{z^D f_i}{n_i^{eff}} + \frac{\langle k_N \rangle}{n_i} \right) \sum_{j=1}^N n_{ij} = \left(\frac{z^D f_i}{n_i^{eff}} + \frac{\langle k_N \rangle}{n_i} \right) n_i. \quad (\text{S.9})$$

And therefore the unperturbed matrix, \mathbf{M}_0 , 's largest eigenvalue will be the largest among them:

$$\Lambda_0^{\max} = \left(\frac{z^D f_i}{n_i^{eff}} + \frac{\langle k_N \rangle}{n_i} \right) n_i \Big|_{\max} = \left(\frac{z^D f_{\max}}{n_{\max}^{eff}} + \frac{\langle k_N \rangle}{n_{\max}} \right) n_{\max}. \quad (\text{S.10})$$

The corresponding right hand side eigenvector's components will all be zero except for those corresponding to the patch with the maximum eigenvalue, which will be 1:

$$(|0^{\max}\rangle)^{i:N+j} = \delta_{i,\max}. \quad (\text{S.11})$$

As for the left-hand side eigenvector, it will read:

$$\left(\langle \tilde{0}^{\max} | \right)_{i:N+j} = \frac{1}{n_{\max}} \delta_{i,\max} n_{ij}, \quad (\text{S.12})$$

where $\frac{1}{n_{\max}}$ acts as a normalization factor.

Furthermore, at first and second order, we can calculate the correction of the eigenvalues Λ_1^i and Λ_2^i as:

$$\Lambda_1^i = \langle \tilde{0}^i | \mathbf{M}_1 | 0^i \rangle \quad (\text{S.13})$$

$$\Lambda_2^i = \langle \tilde{0}^i | \mathbf{M}_1 | 1^i \rangle + \langle \tilde{0}^i | \mathbf{M}_2 | 0^i \rangle. \quad (\text{S.14})$$

Where, for a non-degenerated eigenvalue, $|1^i\rangle$ reads:

$$|1^i\rangle = \sum_{p \neq i} \frac{\langle \tilde{0}^p | \mathbf{M}_1 | 0^i \rangle}{\Lambda_i^0 - \Lambda_p^0} |0^p\rangle. \quad (\text{S.15})$$

Thus, for the largest eigenvalue:

$$\begin{aligned} \langle \tilde{0}^{\max} | \mathbf{M}_1 | 0^{\max} \rangle &= \sum_{i,j} \langle \tilde{0}^{\max} |_{i,N+j} (\mathbf{M}_1 | 0^{\max} \rangle)^{i:N+j} \\ &= \sum_{i,j} \frac{n_{ij}}{n_{\max}} \delta_{i,\max} \left(\frac{z^D f_i}{n_i^{\text{eff}}} n_{\max i} + \frac{z^D f_{\max}}{n_{\max}^{\text{eff}}} (-2\delta_{\max,i} + \delta_{\max,j}) n_{\max} + \right. \\ &\quad \left. + c_{\text{sat}} \sum_k n_{\max k} T_{jk}^{i \max} \right) = \sum_j \frac{n_{\max j}}{n_{\max}} \left(\frac{z^D f_{\max}}{n_{\max}^{\text{eff}}} n_{\max \max} + \right. \\ &\quad \left. + \frac{z^D f_{\max}}{n_{\max}^{\text{eff}}} (-2 + \delta_{\max,j}) n_{\max} + c_{\text{sat}} \sum_k n_{\max k} T_{jk}^{\max \max} \right) \\ &= \frac{z^D f_{\max}}{n_{\max}^{\text{eff}}} (R_{\max,\max} n_{\max} + n_{\max \max} - 2n_{\max}) + \\ &\quad + \frac{c_{\text{sat}}}{n_{\max}} \sum_{j,k} n_{\max j} n_{\max k} T_{jk}^{\max \max} \\ &= 2z^D f_{\max} \frac{n_{\max}}{n_{\max}^{\text{eff}}} (R_{\max,\max} - 1) + \frac{c_{\text{sat}}}{n_{\max}} \sum_{j,k} n_{\max j} n_{\max k} T_{jk}^{\max \max}. \end{aligned}$$

Where $R_{\max,\max} = n_{\max \max} / n_{\max}$ is the *autoloop* fraction at the most vulnerable patch. Note that the first term corresponds to the first-order correction to the largest eigenvalue when in-transit contagion is not considered.

As for the second-order correction to the largest eigenvalue, we have that:

$$\langle \tilde{0}^p | \mathbf{M}_1 | 0^{\max} \rangle = \frac{z^D f_p}{n_p^{\text{eff}}} n_{\max p} + \frac{z^D f_{\max}}{n_{\max}^{\text{eff}}} (-2\delta_{\max p}) + \frac{z^D f_{\max}}{n_{\max}^{\text{eff}}} \frac{n_{p \max}}{n_p} + \frac{c_{\text{sat}}}{n_p} \sum_{j,k} n_{p j} n_{\max k} T_{jk}^{p \max}. \quad (\text{S.16})$$

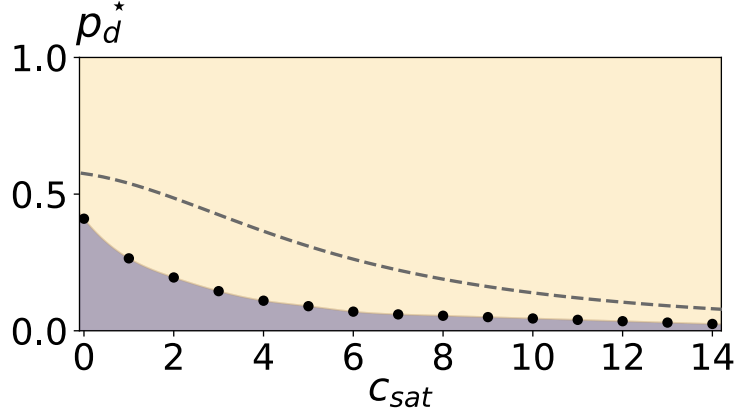
$$\langle \tilde{0}^{\max} | \mathbf{M}_1 | 0^p \rangle = \frac{z^D f_{\max}}{n_{\max}^{\text{eff}}} n_{p \max} + \frac{z^D f_p}{n_p^{\text{eff}}} (-2\delta_{\max p}) + \frac{z^D f_p}{n_p^{\text{eff}}} \frac{n_{\max p}}{n_{\max}} + \frac{c_{\text{sat}}}{n_{\max}} \sum_{j,k} n_{\max j} n_{p k} T_{jk}^{\max p}. \quad (\text{S.17})$$

$$\langle \tilde{0}^{\max} | \mathbf{M}_2 | 0^{\max} \rangle = \frac{z^D f_{\max}}{n_{\max}^{\text{eff}}} n_{\max} + \sum_j \frac{z^D f_j}{n_j^{\text{eff}}} \frac{(n_{\max j})^2}{n_{\max}}. \quad (\text{S.18})$$

All expressions derived above can be further simplified by considering that, for the values of p_d at which the perturbative expansion (to second order) remains valid, we can approximate $n_i \approx n_i^{\text{eff}}$. Under this assumption, the terms in the expansion of the spectral radius of the mixing matrix become:

$$\Lambda_0^{\max} \approx z^D f_{\max} + \langle k_N \rangle, \quad (\text{S.19})$$

$$\Lambda_1^{\max} \approx 2z^D f_{\max} (R_{\max,\max} - 1) + \frac{c_{\text{sat}}}{n_{\max}} \sum_{j,k} n_{\max j} n_{\max k} T_{jk}^{\max \max}, \quad (\text{S.20})$$



Supplementary Fig. 1. Impact of c_{sat} on epidemic detriment: comparison between numerical and perturbative results. The mobility value p_d^* , defined as the value of p_d that maximizes the epidemic threshold λ_c , is plotted as a function of c_{sat} . Numerical results are shown as black dots, while the dashed line corresponds to the prediction from the perturbative expression given in Eq. (S.22). Shaded regions indicate distinct dynamical regimes: in light purple, increasing mobility enhances the epidemic threshold, whereas in light yellow, mobility reduces λ_c . Simulations are performed with parameters $K = 10^{-3}$, $\langle k_D \rangle = 8$, and $\langle k_N \rangle = 3$.

$$\begin{aligned} \Lambda_2^{\max} \approx & \sum_{p \neq \max} \frac{\left[\frac{z^D f_p}{n_p} n_{\max p} + \frac{z^D f_{\max}}{n_{\max}} \frac{n_p \max}{n_p} + \frac{c_{sat}}{n_p} \sum_{j,k} n_{pj} n_{\max k} T_{jk}^{p \max} \right]}{z^D (f_{\max} - f_p) + z^N (\sigma_{\max} - \sigma_p)} \\ & \times \left[\frac{z^D f_{\max}}{n_{\max}} n_{p \max} + \frac{z^D f_p}{n_p} \frac{n_{\max p}}{n_{\max}} + \frac{c_{sat}}{n_{\max}} \sum_{j,k} n_{\max j} n_{pk} T_{jk}^{\max p} \right] \\ & + z^D f_{\max} + \sum_j \frac{z^D f_j}{n_j} \frac{(n_{\max j})^2}{n_{\max}}. \end{aligned} \quad (\text{S.21})$$

This perturbative analysis of the epidemic detriment phenomenon in the low-mobility regime, reveals that to first order, the detriment is primarily driven by the reduction in contacts between residents of the most vulnerable patch. Furthermore, the positive term in Eq. (S.19) shows that in-transit contagion counteracts epidemic detriment by increasing interactions between residents of the most vulnerable node. Importantly, this counter-detriment effect emerges at first order when assuming $c(p_d) \approx c_{sat}$ as we have done here, and at second order when a Hill function is used to model *in itinere* contacts.

Having now an explicit expression for the spectral radius of the mixing matrix, we can derive a fully analytical expression for the epidemic threshold. Furthermore, by differentiating this expression and setting the derivative to zero, we obtain an analytical estimate for p_d^* , the mobility level at which the epidemic threshold reaches its maximum. This marks the turning point beyond which the phenomenon of epidemic detriment begins to subside:

$$\frac{\partial \beta_c}{\partial p_d} = \frac{\partial}{\partial p_d} \left(\frac{\mu}{\Lambda_0^{\max} + p_d \Lambda_1^{\max} + p_d^2 \Lambda_2^{\max}} \right) = 0 \implies p_d^* = \frac{-\Lambda_1^{\max}}{2\Lambda_2^{\max}}. \quad (\text{S.22})$$

To round off the analysis, Supplementary Fig. 1 presents a comparison between the values of p_d^* obtained numerically and those predicted analytically by the perturbative expression in Eq. (S.22). As expected, the agreement improves for higher values of c_{sat} , which corresponds to a weaker epidemic detriment effect and lower values of p_d^* . In such regimes, the system remains closer to the assumptions underlying the perturbative approach—particularly the dominance of the zeroth- and first-order terms—thus enhancing the accuracy of the analytical prediction.